Structural polymorphism correlated to surface charge in filamentous bacteriophages

S. Bhattacharjee,* M. J. Glucksman,* and Lee Makowski‡

*Department of Biochemistry and Molecular Biophysics, College of Physicians and Surgeons, Columbia University, New York, New York 10032 USA; and ‡Department of Physics, Boston University, Boston, Massachusetts 02215 USA

ABSTRACT Fiber diffraction studies are used to demonstrate that changes in the helical symmetry of the protein coat of filamentous bacterial viruses fd and M13 are correlated with changes in the surface charge. Comparison of the structure of M13 and fd at pH 2 and 8 indicate that surface charge affects both the helical symmetry and flexibility of the virions. The changes in helical symmetry are similar in magnitude to that observed in the *Pseudomanas* phage Pf1 and probably reflect an inocuous side effect of the particle flexibility required for protection of the virus particles from damage due to shear. The magnitude of the observed changes in helical symmetry appears to be limited to that which can occur without repacking of the interfaces between the α-helices making up the viral protein coat.

INTRODUCTION

M13 and fd are filamentous bacteriophages differing by less than 2% in nucleotide sequence and with coat proteins differing by only a single amino acid; asn_{12} of M13 corresponds to asp_{12} in fd. These viruses are single-stranded DNA phage composed of a closed, circular, single-stranded DNA molecule packaged into a flexible, filamentous particle 65 Å in diameter and ~9,300 Å in length (for reviews, see Makowski, 1984; Model and Russel, 1988). The particle is composed largely of ~2,800 copies of a small, largely hydrophobic coat protein that forms a cylindrical shell about the DNA. The coat protein is 50 amino acids in length and consists mainly of a single, gently curving α-helix tilted at an angle of ~20° to the viral axis (Marvin, 1966; Opella et al., 1987; Glucksman, 1990; Glucksman et al., 1992). A diagram of the structural organization of the virus is shown in Fig. 1.

The symmetry of the protein coat combines a fivefold rotation axis with an approximate two-fold screw axis (Makowski and Caspar, 1981; Banner et al., 1981). In this paper we will use the notation $C_5S_{2.0}$ to designate the symmetry of a helical object exhibiting fivefold cyclic (rotational) symmetry and a twofold screw. The elements of this helical symmetry, and their relation to the corresponding fiber diffraction patterns are described in Fig. 2. The origin of layer line splitting, an experimental measure of deviations from the twofold screw symmetry is also described in this figure.

The similar *Pseudomanas* phage Pf1 has its subunits arranged on a one-start helix with 5.40 subunits per turn, or a symmetry of $C_1S_{5.40}$. This phage has been shown to undergo a symmetry transition at about 8°C (Wachtel et al., 1976; Nave et al., 1979; Hinz et al., 1980). As temperature decreases, the helical symmetry changes from $C_1S_{5.40}$ to $C_1S_{5.46}$. Heavy atom binding also affects the helical symmetry of the phage particle. These symmetry transitions may represent an innocuous side effect of the particle flexibility that provides critical protection of the particles from damage due to shear (Makowski, 1984; Nambudripad et al., 1991).

Symmetry transitions have not been reported for M13. Differential scanning calorimetry (Hinz et al., 1980) indicated that a temperature transition similar to that of Pf1 does not occur in fd. Heavy atom derivatives of M13 also have essentially the same symmetry as native M13 (Glucksman et al., 1992). However, data have been reported that are consistent with slight variations in the $C_5S_{2.0}$ symmetry for fd and the similar phage particles If1 and IKe (Marvin et al., 1974). Here we describe a systematic survey of symmetry changes that occur in the class I (fd-like) filamentous bacteriophage particles.

MATERIALS AND METHODS

Specimen preparation

M13 and fd were grown and purified using standard techniques (e.g., Maniatis et al., 1982) as reported previously (Glucksman, 1990; Glucksman et al., 1992). Virus strains were obtained from Dr. Peter Model (Rockefeller Univ.) and Dr. Stan Opella (Univ. of Pennsylvania). A coat protein mutant of fd with tyr_{24} replaced by phe_{24} (fd24f) was provided by Dr. Opella.

After isolation on either a CsCl or KBr step gradient, the purified

*Dr. Glucksman's current address is Dr. Arthur M. Fishman Research Center in Neurobiology, Mount Sinai School of Medicine, One Gustave L. Levy Place, New York, New York 10029 USA.

0006-3495/92/03/725/11 $2.00

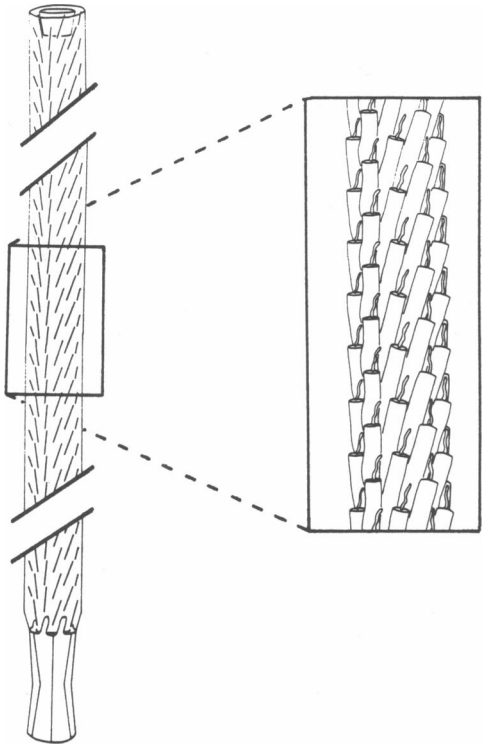

FIGURE 1 The virions of M13, fd, and f1 are virtually identical. They are made up of ~2,800 copies of the gene 8 protein, the major coat protein, and 5 copies each of 4 minor proteins. Two minor proteins, gene 7 and gene 9 proteins, form a plug at one end of the virion (*top in this diagram*), and are active in the initiation of the assembly of the virus particle. Gene 6 and gene 3 proteins make up a host cell recognition complex at the other end of the virion (*bottom in this figure*). The gene 8 protein is made up of 50 amino acids and consists of a single, gently curving α-helix extending from pro_6 to the carboxy terminus (*inset*). The first five amino acids are flexible in solution.

virus was dialyzed against tris-HCl (pH 8.0) and then centrifuged for 45 min at 37,000 *g* to remove large aggregates. For specimens prepared at pH 2, the virus was dialyzed against 25 mM disodium citrate buffer (pH 2.0). The viruses were then pelleted at 150,000 *g* for 150 min and the pellets resuspended with a small amount of supernatant to a concentration of 75 mg/ml. Virus concentration was determined by measuring absorbance at 268 nm using an extinction coefficient of 3.84 $mg^{-1}cm^2$.

Fibers of virus particles were oriented in a magnetic field using techniques similar to those described in detail by Nave et al. (1981). A 10–20-μl drop of purified virus was placed between the tips of two 1-mm diameter glass rods spaced 1 mm apart. The glass rods are prepared with blunt, slightly curved ends. They are treated with a siliconizing agent and the silicon coating is removed from the tips by gentle rubbing with emory paper. Once the drop of virus solution is suspended between the glass rods, the entire assembly is sealed in a 1-cm diameter test tube equilibrated at a nominal relative humidity of 100%, and containing a reservoir of distilled water. The test tube is then placed in the bore of a 5.8 Tesla superconducting magnet at 20°C. The fibers were slowly dehydrated over a period of 4–6 wk by gradually increasing the temperature. Fibers were dehydrated rapidly over a period of 3–6 d by exchanging the distilled water reservoir in the test tube with a saturated salt solution with a vapor pressure corresponding to 93% relative humidity. This partial dehydration increased the viscosity of the virus solution so that magnetically induced virus orientation was maintained after removal of the fiber from the magnet. The solvent content of the partially dried fibers was always greater than ~35% (Specthrie et al., 1986). The resulting fibers were removed from the test tube and mounted in thin walled glass or quartz capillaries in vapor equilibrium with a small reservoir of mother liquor.

X-ray diffraction

X-ray diffraction patterns were obtained using radiation from a rotating anode source (Rigaku USA Inc. RU-200; Danvers, MA) with double mirror focussing optics (Phillips and Rayment, 1985) or monochromated synchrotron radiation from the A-1 experimental station at the Cornell High Energy Synchrotron Source (CHESS). Exposure times were usually 24–48 h using the rotating anode source or 3–6 min using the synchrotron source. A wavelength of 1.54 A was used for all experiments. Specimen-to-film distances were usually 6–8 cm.

Selected films were densitometered using an Optronics P-1000 scanning microdensitometer or an Eikonix Corp. digital camera (Bedford, MA). Data were averaged on a 50-μm square raster and displayed as contour plots for the identification and measurement of peak locations.

RESULTS

X-ray diffraction patterns

X-ray diffraction patterns from four fibers are shown in Fig. 3. Fig. 3 *a* is a diffraction pattern from M13 at pH 2. Fibers prepared at pH 2 were uniformly well oriented and exhibited well defined layer lines spaced at intervals corresponding to an axial repeat of 33.1 A. Measurable intensity often extended off the edge of the film at spacings of 3 A or better. No layer line splitting could be detected. The symmetry of the particles giving rise to these diffraction patterns is $C_5S_{2.0}$ (Makowski and Caspar, 1981; Banner et al., 1981). X-ray diffraction patterns from M13, fd, and fd24f at pH 2 were indistinguishable. Fig. 3 *b* is a diffraction pattern from M13 at pH 8. The orientation of particles in the fiber used to obtain the pattern is not as good as for the specimen at pH 2 shown in Fig. 3 *a*. Careful examination of the first layer line indicates that a very small amount of layer line splitting may be occuring, but this is not evident in all patterns from M13 at pH 8. The symmetry of particles in this fiber is very close to $C_5S_{2.0}$, but not precisely so. Fig. 3 *c* is a diffraction pattern from fd at pH 8, and Fig. 3 *d* is a pattern from fd24f at pH 8. Both of these patterns exhibit extensive layer line splitting, most obvious on the first layer line, but also visible on layer lines 2, 3, and 4. On the equator, the layer line splitting is necessarily up–down symmetric. This led Banner et al. (1981) to

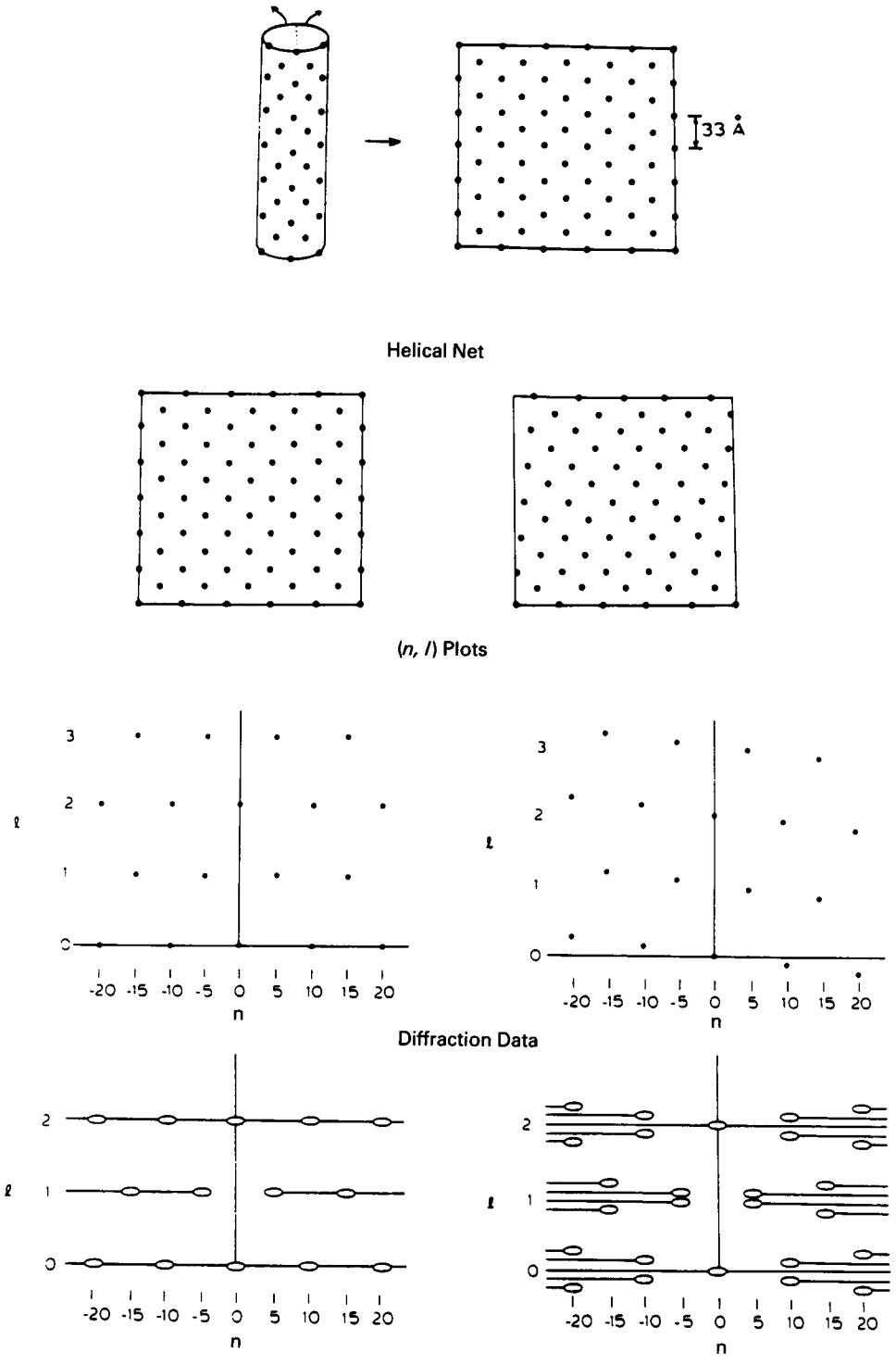

FIGURE 2 Diagrams representing the helical symmetry and diffraction patterns for objects with exact twofold screw symmetry (left) and a 2.08-fold screw (*right*). The helical symmetry of M13 (fd, f1) is most readily displayed as a helical net as in the top portion of this diagram. A helical net is a map of equivalent points in a helix made by making a vertical cut in a cylinder concentric with the axis of the helix, and opening up the cylinder. The positions of Bessel function terms in a fiber diffraction pattern from a helical object are represented in (n, l) plots (*middle*). The twisting of the helix from a 2.0-fold screw to a 2.08-fold screw causes the Bessel function terms to shift up and down. The actual fiber diffraction pattern from a helix has a close relationship to the (n, l) plot. The positions of reflections in the diffraction patterns are represented by a right–left and up–down averaging of the (n, l) plot, resulting in a distribution of reflections as in the bottom diagrams here.

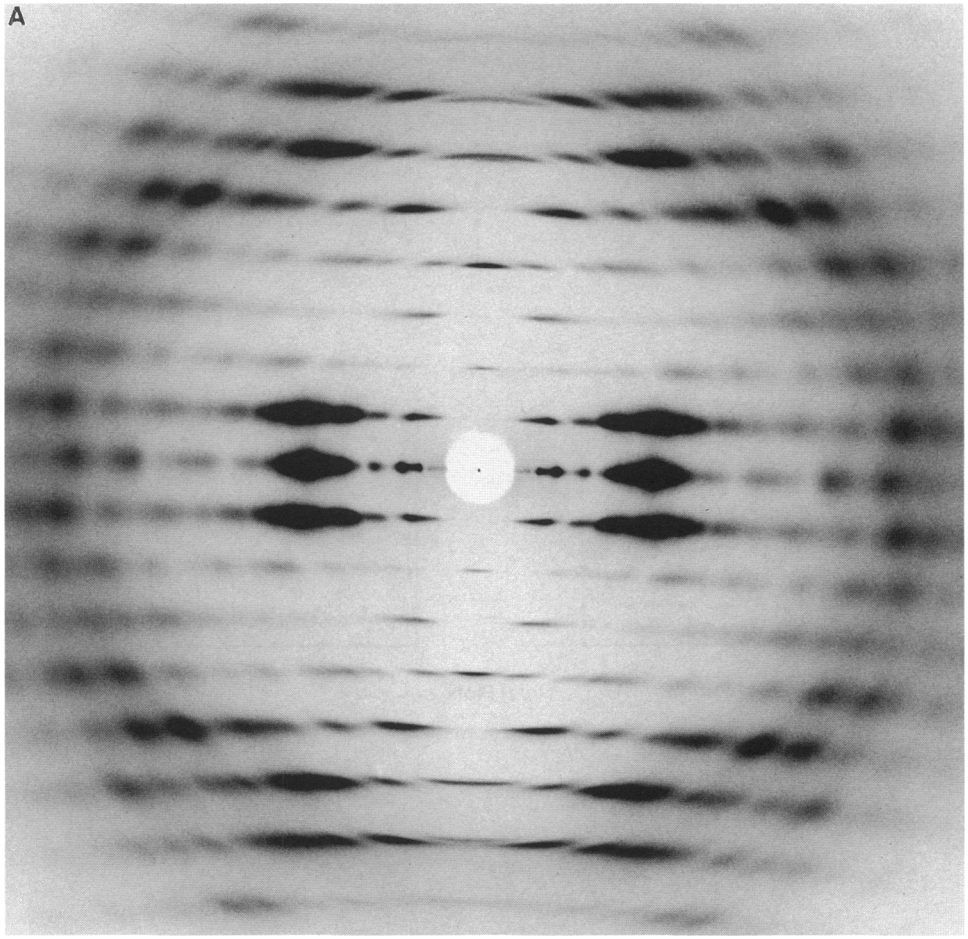

FIGURE 3 Diffraction patterns from magnetically oriented fibers of filamentous bacteriophages. (*a*) M13 at pH 2. (*b*) M13 at pH 8. (*c*) fd at pH 8. (*d*) fd24f at pH 8.

interpret these patterns as due to "double-orientation" of particles in the fiber. However, the splitting on the off-equatorial layer lines is clearly not up–down symmetric, indicating that a more complex phenomenon is leading to the observed diffraction.

The diffraction patterns in Fig. 3 are representative of dozens of patterns taken from these viruses at pH 2 and pH 8. At pH 2, none of the viruses give rise to diffraction patterns that exhibit layer line splitting. At pH 8, diffraction patterns from fd and fd24f always exhibit splitting. Diffraction patterns from fibers of M13 at pH 8 that were formed very slowly (4–6 wk) exhibit very little or no observable splitting. When fibers of M13 are dried in 3–6 d, they usually exhibit splitting comparable to that seen for fd at pH 8. These results are summarized in Table 1.

Fig. 4 is a contour plot of the optical densities in a diffraction pattern from fd24f. It is clear from this diagram that the intensity along the layer line has broken into a number of layer lines parallel to one another and spaced approximately equidistant from one another. Fig. 5 is a diagram of the positions of reflections in the split first layer lines in patterns from (*a*) fd and (*b*) fd24f. Table 2 includes a list of the reflections diagrammed in Fig. 5.

Layer line splitting

The diagrams in Fig. 2 provide a qualitative description of the origin of layer line splitting. For particles with an exact twofold screw axis, the cyclic Fourier components corresponding to 0-, 10-, 20- . . . fold rotational symmetry fall exactly on the equator. Similarly, components corresponding to projections down 5-, 15-, 25- . . . start helices fall precisely on the first layer line. If the particle is then twisted slightly, changing its twofold screw axis to a nonintegral screw axis, the nonzero cyclic terms shift up and down from the equator, and all terms shift from the

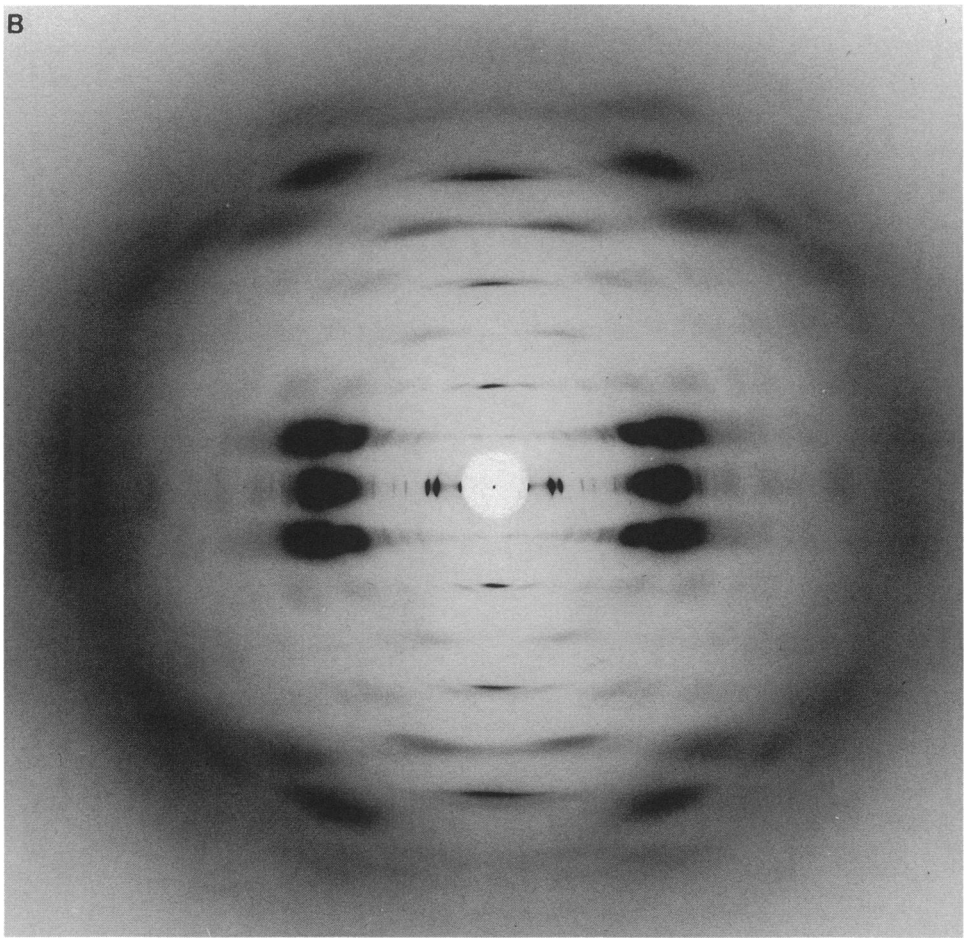

FIGURE 3 (continued)

first layer line. The observed shifts can be used to calculate the change in screw axis. For this calculation, we used data from the equator and first layer lines. The average position of the first layer line is estimated from the position of the meridional peak on the second layer line (which corresponds to a cylindrically symmetric [zero-order] rotational term that is not directly affected by changes in the screw axis). Peaks observed on the first layer line were assigned a helical order of ±5, ±15, or ±25 depending on their distance from the average position of the first layer line. Although every observed peak may correspond to a composite of intensities from adjacent layer lines (see, e.g., Stubbs and Makowski, 1982) the split layer line positions are well separated relative to the degree of disorientation. This means overlap of adjacent layer lines may result in slight deviation of the peaks from their expected positions (as seen in Fig. 5), but is unlikely to result in an incorrect indexing of the peaks. Defining Δ as the meridional separation between Bessel function terms differing in order by ±10, we calculated the symmetry of the particles giving rise to the observed diffraction as described in Fig. 6. A summary of these results appears in Table 3.

This analysis provides us with a basis for reanalyzing the results of Marvin et al. (1974), which included several diffraction patterns with data indicative of layer line splitting in fd or similar viruses. The diffraction patterns presented in that work were taken before the discovery (Torbet and Maret, 1979) that magnetic fields could be used to greatly improve the orientation of filamentous phage particles in fibers. Consequently, the errors in the helical symmetry derived from those patterns will be larger than for those diffraction patterns reported here. Marvin et al. (1974) identified strong, near meridional intensity on the first layer line and recognized that the strong intensity in the 10-A region was shifted axially relative to it. Comparing them to the diffraction patterns in Fig. 3, it appears that Marvin et al. (1974) observed the +5 and −15 terms, and in some

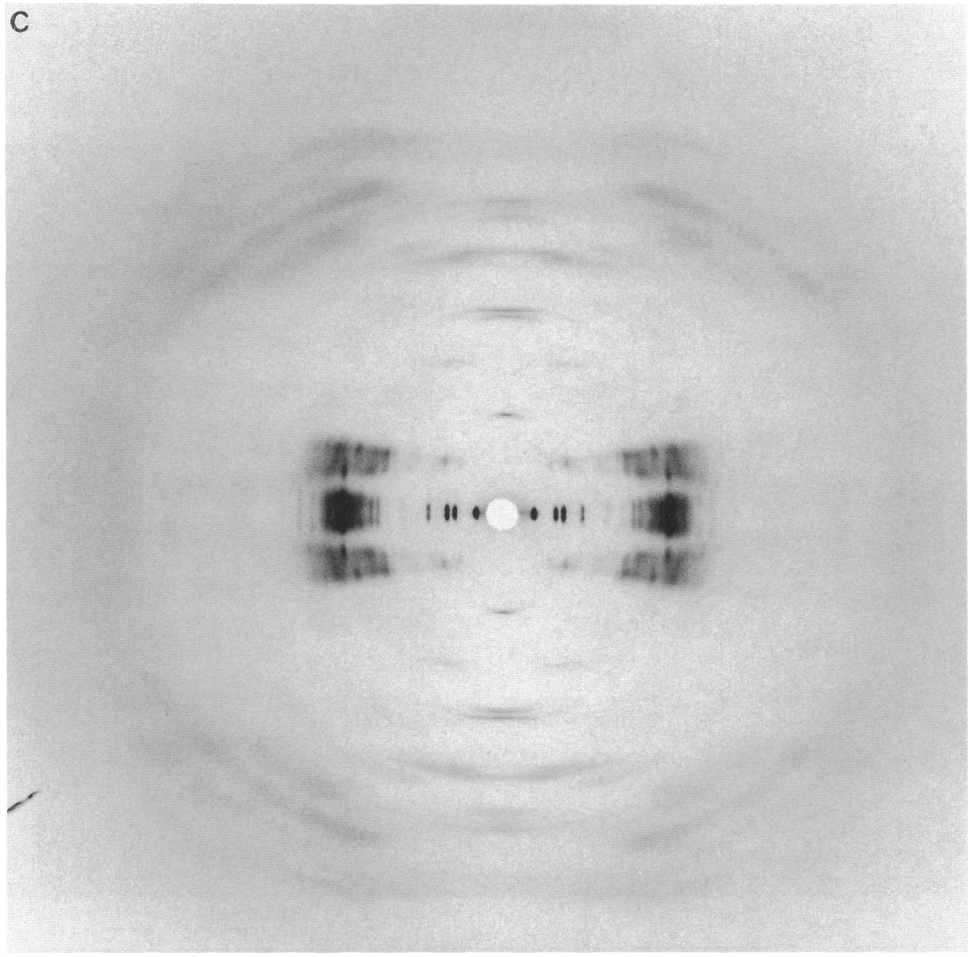

FIGURE 3 (continued)

patterns, may have identified other intermediate terms. Using this assignment, we recalculated the symmetry of the particles giving rise to the diffraction patterns reported in that study. The results are summarized in Table 4. The symmetry changes calculated from those diffraction patterns are very similar to those calculated for fd from patterns like that in Fig. 3 *c*. They suggest that fd, IKe, and If1 have very similar, if not identical symmetries at pH 8.

Helical aggregates

Although a slight change in the helical symmetry of the diffracting particles explains the splitting of layer lines, it does not explain the observed positions of reflections relative to the meridian, nor the sharpness of the reflections, which, in these patterns is suggestive of highly ordered packing of viruses in the fiber. In diffraction from a helical object, a Bessel function term of order, n, is insignificant closer to the meridian than a distance, R_{min}, where

$$R_{min} = (n + 2)/2\pi r_{max},$$

and r_{max} is the maximum radius of the object giving rise to the diffraction. Given the closest approach a Bessel order term makes to the meridian (R_{min}), this relation can be used to calculate the radius (r_{max}) of structural features giving rise to it. In Table 2, values of r_{max} calculated from the observed reflections on the first layer lines are listed. The calculated r_{max} values are as large as 100 A (much larger than the 33 A outside radius for a single virus particle).

The most likely explanation for this observation is the formation of large, helical aggregates of the virus particles in the specimens. This would also explain the sharpness of reflections in these patterns. A number of

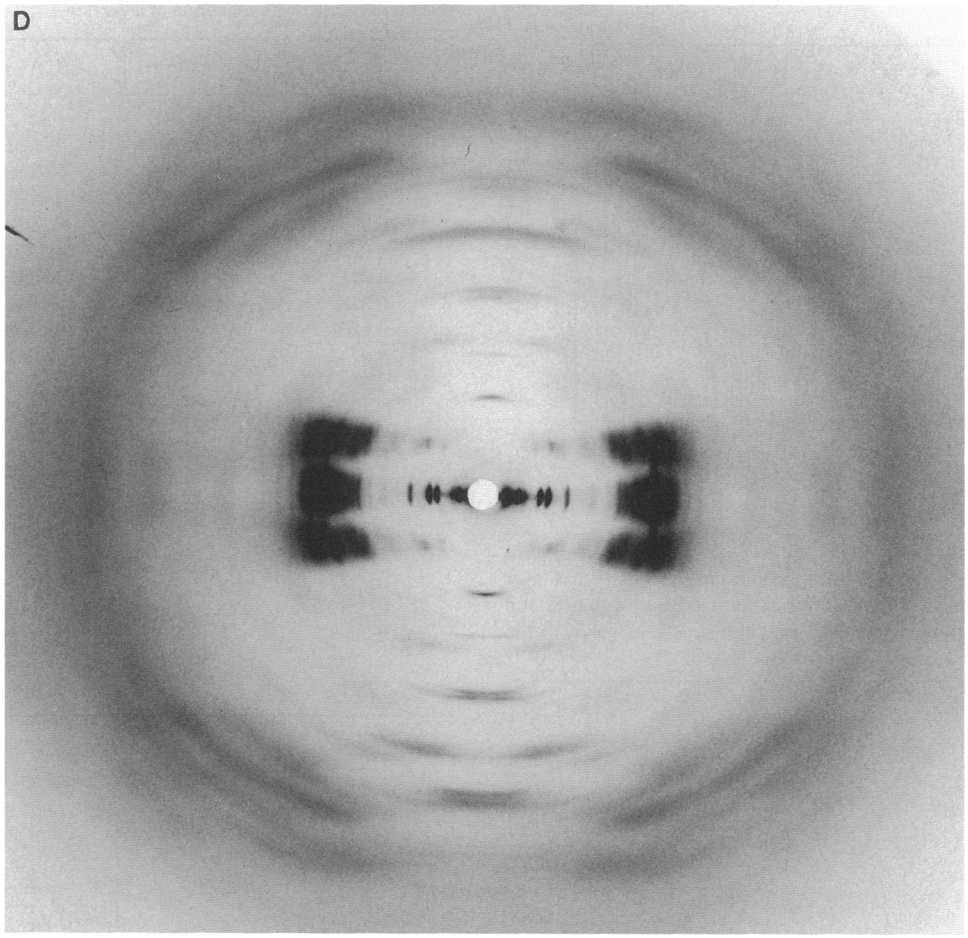

FIGURE 3 (continued)

helical macromolecular assemblies are known to form helical aggregates, including sickle-cell hemoglobin double-strands (Magdoff-Fairchild and Chiu, 1979; Vassar et al., 1982; Potel et al., 1984), and fibrinogen (Weisel et al., 1987). When helical objects aggregate through the formation of regular, side-to-side interactions, they form aggregates with the same pitch as that of the individual constituent particles. The form of the diffraction data from fd and fd24f indicates that helical aggregates have formed within the fiber during drying. This has no bearing on the calculation of the helical pitch of individual particles because the pitch of the aggregate is identical to the pitch of the constituent particles.

TABLE 1 Layer line splitting in diffraction patterns from filamentous bacteriophages

	fd	fd24f	M13
pH 2	–	–	–
pH 8 (slow)	+	+	–
pH 8 (fast)	+	+	+

At pH 2 all viruses exhibit an exact twofold screw axis. At pH 8, in fibers formed in under a week, all viruses exhibited layer line splitting diagnostic of deviation from an exact twofold screw axis. At pH 8, in fibers formed very slowly, differences in observed virus particle symmetry were correlated with the surface charge of the particle.

DISCUSSION

The α-helical subunits of M13 lie approximately parallel to the 15-start helices at the surface of the virus particle as illustrated in Fig. 1. Since these helices are tightly packed in the virus particle, a change in the helical symmetry of the particle reflects a change in the tilt of these helices. Conversely, changes in the interactions of the helices near the particle's surface may be responsible for the observed change in the helical symmetry of the particle.

The results presented here indicate that the helical

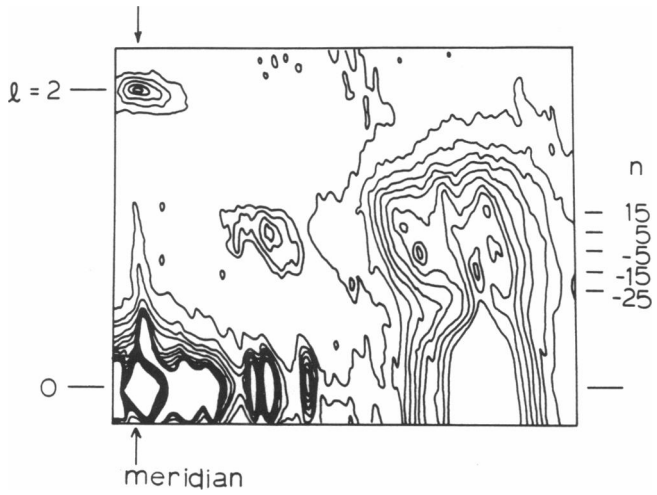

FIGURE 4 Contour plot of optical densities in a diffraction pattern from fd24f at pH 8 in which the splitting of intensities on the first layer line can be clearly seen. The positions of the meridian, equator, and layer line 2 are marked. The Bessel function orders assigned to the intensities on the first layer line are also indicated.

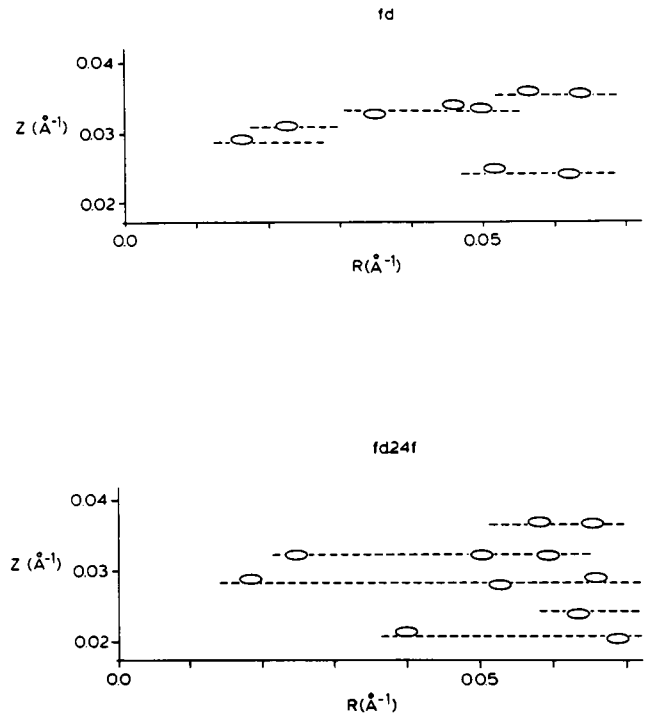

FIGURE 5 Diagrams of the positions of reflections on the first layer lines of diffraction patterns from (*a*) fd and (*b*) fd24f. Dashed lines are equispaced to emphasize the breaking up of intensity into well defined Bessel order terms.

TABLE 2 Positions of reflections of layer line 1

$Z(A^{-1})$	n	$R(A^{-1})$	$r(A)$
fd (ph 8)			
0.0359	25	0.0640	67.1
0.0362	25	0.0566	76.7
0.0337	15	0.0498	54.3
0.0343	15	0.0461	58.7
0.0328	15	0.0350	77.3
0.0313	5	0.0227	44.8
0.0291	−5	0.0164	62.1
0.0251	−25	0.0519	82.8
0.0243	−25	0.0622	69.1
fd24f (pH 8)			
0.0364	15	0.0655	41.3
0.0367	15	0.0582	46.4
0.0319	5	0.0595	17.1
0.0321	5	0.0504	20.2
0.0323	5	0.0247	41.2
0.0285	−5	0.0659	15.4
0.0277	−5	0.0528	19.3
0.0287	−5	0.0185	55.0
0.0240	−15	0.0635	42.6
0.0206	−25	0.0689	62.4
0.0216	−25	0.0403	106.6

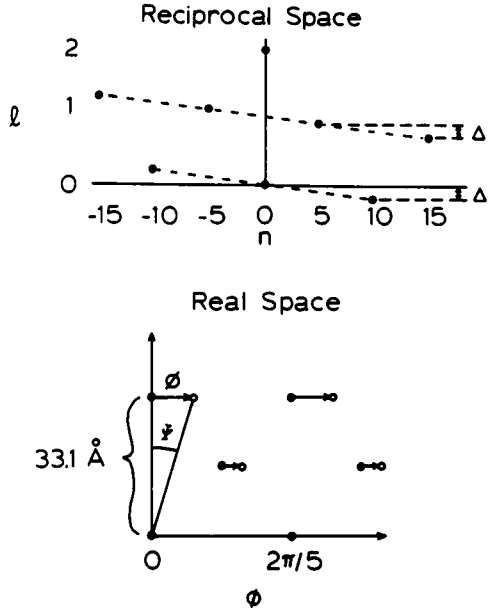

FIGURE 6 Definition of Δ, ϕ, and Ψ. The experimental measurement is Δ as determined by the magnitude of the layer line splitting (*top diagram*). The structural parameters, Ψ (the change in tilt of the J_{10} Bessel order term) and ϕ (angular rotation of the units displaced by 33.1 A relative to one another) are determined by:

$$\phi = (c\Delta/2)(2\pi/5)$$

$$\Psi = \mathrm{Tan}^{-1}(\phi r/c)$$

where r is the radius at which Ψ is calculated, and c is the axial repeat (~33 A for most of these virus specimens).

TABLE 3 **Calculated symmetry of phage particles**

	fd (pH 8)	fd24f (pH 8)
Δ	0.0023 A^{-1}	0.0042 A^{-1}
Φ	2.69°	5.00°
Pitch	4425 A	2381 A
Ψ*	2.44°	4.53°
Symmetry	$C_5S_{2.04}$	$C_5S_{2.07}$

*Based on a radius of 30 A.

symmetries of filamentous bacteriophages M13 and fd are sensitive to pH between pH 2 and 8. The ionic properties of filamentous phage particles are completely determined by the titrating groups in the amino terminal half of the coat protein (Zimmermann et al., 1986). These groups are on the surface of the virus particle. Charged groups near the carboxyl terminus interact with the DNA (Hunter et al., 1987; Rowitch et al., 1988), and apparently have no effect on the ionic properties of the virions. On the viral surface, the M13 coat protein has four acidic residues, one basic residue and the positively charged amino terminus. In fd, there is an additional acidic group, asp_{12}. In going from pH 2 to pH 8, the surface charge of the M13 coat protein goes from approximately +2 to −2. In fd it changes from about +2 to −3. At pH 2, both the charge per protein and the helical symmetry are the same for fd and M13. At pH 8, fd has one additional negative charge per coat protein, and exhibits different behavior from M13 with regard to the observed helical symmetry. The mutant fd24f has the same surface charges as fd, identical symmetry at pH 2 and similar, though not identical, symmetry at pH 8. These results indicate that surface charge is a major factor, but not the only factor, in stabilizing the helical symmetry of the phage particle.

The effect of drying speed on the observed layer line splitting in M13 indicates that the helical symmetry may be affected by additional properties of the coat proteins. Aggregates of regularly interacting helical particles exhibit the same pitch as the constituent particles (Makowski and Fairchild, 1986; Weisel et al., 1987). If the helical particles are of fixed pitch, radial growth of the aggregate is limited; as growth proceeds, the added filaments are increasingly distorted in order to conform to the helical twist of the aggregate. At some point, the energy required to distort the particles being added exceeds that obtained from binding energy and the radial growth ceases (Makowski and Fairchild, 1986). This behavior is consistent with the observations of diffraction from fibers of fd and fd24f, but not from fibers of M13.

TABLE 4 **Calculation of pitch from observations of Marvin et al. (1984)**

Virus	Axial repeat reported	Calculated pitch	Source
If1	210	4,200	Plate VI
If1	207	4,140	Plate VII
fd	208	4,160	Fig. 1
IKe	213	4,260	Fig. 3
fd	410–416*	4,100–4,160	Fig. 4
If1	205–206	4,100–4,120	Fig. 5

*Marvin et al. (1984) probably also saw the J_{-5} term in this pattern as well as the J_5 and J_{-15} terms observed for all the other patterns.

As a fiber of M13 at pH 8 slowly dries, helical aggregates of M13 form. If drying proceeds slowly enough, the aggregates get very large and appear to untwist until the particles have an almost exact twofold screw axis. In this case, growth of aggregates is not limited by fixed helical symmetry. Binding energy that leads to distortion of particles on the surface of the aggregate appears to provide energy for the progressive untwisting of the aggregates. Optical microscopy of concentrated solutions of M13 has been used to demonstrate the formation of helical aggregates which, during growth, increase in both pitch and radius (Hellman, 1990; Hellman and Makowski, unpublished results). The pitch of these aggregates is measured in microns by the time they are large enough to be observed by optical microscopy, and the ionic strength in these solutions is lower than in the fibers. Nevertheless, they may represent either a very similar process to that reported here, or the final stages in the growth of helical aggregates during fiber formation. Significantly, in those studies, no aggregates formed at pH 2 exhibited visible twist (Hellman, 1990).

Based on these observations, we have developed the following model to account for the diffraction data from M13 and fd: At pH 2, both fd and M13 have twofold screw axes, and the entire diffraction pattern may be accounted for based on a particle symmetry $C_5S_{2.0}$. At pH 8, because of the change in surface charges, fd takes on a helical symmetry of $C_5S_{2.04}$. During formation of fibers the fd particles form helical aggregates of limited radial extent, but their helical symmetry does not change substantially during fiber formation. This is also true of fd24f which has a helical symmetry $C_5S_{2.07}$ at pH 8, deviating from a twofold screw axis by somewhat more than fd. At pH 8, the helical symmetry of M13 also deviates from a simple twofold screw. However, if fiber formation is sufficiently slow, interparticle interactions tend to untwist the M13 particles so that their exact symmetry in the partially dried fiber depends on the radial extent of the helical aggregates formed during dehydration. Slow drying results in the complete untwisting of the particles so that no layer line splitting is observed and the particle symmetry is $C_5S_{2.0}$. Relatively

fast drying (3 to 6 d) does not provide time for the growth of aggregates large enough to completely untwist the particles, and layer line splitting comparable to that of fd is observed. Presumably, the difference of one charge per coat protein alters either the interparticle interactions, particle flexibility, or both, accounting for the different behaviors of M13 and fd.

The changes in helical symmetry reported here are similar in magnitude to those observed for Pf1 on binding of heavy atoms, or reduction of temperature below 8°C. In those transitions, the helical symmetry of Pf1 varied from $C_1S_{5.40}$ to $C_1S_{5.46}$. Here we have reported symmetry changes in M13 and fd from $C_5S_{2.0}$ to $C_5S_{2.07}$. The similar extent of these transitions driven by different forces may be due to limitations in the allowed movement of protein–protein interfaces. Relative displacements of interacting α-helices by less than 1.5 A may be accomplished without repacking of the amino acid side chains of the interface (Chothia et al., 1983). Relative displacement by more than 1.5 A usually requires a repacking of the interface and may require substantially more energy to accomplish.

The largest protein–protein motion observed in the symmetry transitions reported here is between the inside of the α-helical subunit near its amino terminus and the underlying α-helix from a symmetrically equivalent subunit 30 A from its amino terminus. Assuming the symmetry changes reflect comparable relative movement of the α-helical segments, the largest relative motion of abutting helices observed in fd is ~0.9 A and in fd24f is ~1.7 A. Both of these movements can be accomplished without repacking of helix–helix interfaces. Consequently, the observed symmetry changes may reflect the maximum structural change possible without repacking of the interior of the viral protein coat. The relatively large changes in helical symmetry can be tolerated only because of the small radius of protein–protein interactions in the virus. This is the structural basis for flexibility in these virus particles.

We thank Drs. Stanley Opella and Peter Model for supplying strains of virus used. We also thank Drs. Keith Moffat and Wilfred Schildekamp for their very kind assistance in taking the diffraction patterns at CHESS.

Work was supported by the National Institutes of Health.

Received for publication 23 August 1991 and in final form 4 November 1991.

REFERENCES

Banner, D. W., C. Nave, and D. A. Marvin. 1981. Structure of the protein and DNA in fd filamentous bacterial virus. *Nature* (*Lond.*). 289:814–816.

Chothia, C., A. M. Lesk, D. D. Dodson, and D. C. Hodgkin. 1983. Transmission of conformational change in insulin. *Nature* (*Lond.*). 302:500–505.

Glucksman, M. J. 1990. Ph.D. Thesis, Columbia University, New York.

Glucksman, M. J., S. Bhattarcharjee, and L. Makowski. 1992. Three-dimensional structure of a cloning vector: x-ray diffraction studies of filamentous bacteriophage M13. *J. Mol. Biol.* In press.

Hellman, A. D. 1990. B.S. Thesis, Boston University.

Hinz, H.-J., K. O. Greulich, H. Ludwig, and D. A. Marvin. 1980. Calorimetric, density and circular dichroism studies of the reversible structural transition in Pf1 filamentous bacterial virus. *J. Mol. Biol.* 144:281–289.

Hunter, G. J., D. H. Rowitch, and R. N. Perham. 1987. Interactions between DNA and coat protein in the structure and assembly of filamentous bacteriophage fd. *Nature* (*Lond.*). 327:252–254.

Magdoff-Fairchild, B., and C. C. Chiu. 1979. X-ray diffraction studies of fibers and crystals of deoxygenated sickle cell hemoglobin. Proc. Natl. Acad. Sci. USA. 76:223–226.

Makowski, L. 1984. Structural diversity in filamentous bacteriophages. *In* The Structures of Biological Macromolecules and Assemblies, Vol. 1, The Viruses. A. McPherson and F. Jurnak, editors. John Wiley and Sons, New York. 203–253.

Makowski, L., and D. L. D. Caspar. 1981. The symmetries of filamentous phage particles. *J. Mol. Biol.* 145:611–617.

Makowski, L., and B. Fairchild. 1986. Polymorphism of sickle cell hemoglobin aggregates: structural basis for limited radial growth. *Science* (*Wash. DC*). 234, 1228–1231.

Maniatis, T., E. F. Fritsch, and J. Sambrook. 1982. Molecular Cloning: A Laboratory Manual. Cold Spring Harbor Laboratory, Cold Spring Harbor, New York.

Marvin, D. A. 1966. X-ray diffraction and electron microscope studies on the structure of the small filamentous bacteriophage fd. *J. Mol. Biol.* 15:8–17.

Marvin, D. A., W. J. Pigram, R. L. Wiseman, E. J. Wachtel, and F. J. Marvin. 1974. Filamentous bacterial viruses. XII. Molecular architecture of the class I (fd, If1, IKe) virion. *J. Mol. Biol.* 88:581–600.

Model, P., and M. Russel. 1988. Filamentous Bacteriophage in The Bacteriophages, Vol. 2. R. Calendar, editor. Plenum Publishing Corp., New York. 375–456.

Nambudripad, R., W. Stark, and L. Makowski. 1991. Neutron diffraction studies of the structure of filamentous bacteriophage Pf1. *J. Mol. Biol.* 220:359–379.

Nave, C., A. G. Fowler, S. Malsey, D. A. Marvin, H. Siegrist, and E. J. Wachtel. 1979. Macromolecular structural transitions in Pf1 bacterial virus. *Nature* (*Lond.*). 281:232–234.

Nave, C., R. S. Brown, A. G. Fowler, J. E. Ladner, D. A. Marvin, A. Provencer, A. Tsugita, J. Armstrong, and R. N. Perham. 1981. Pf1 bacterial virus. X-ray fiber diffraction analysis of two heavy atom derivatives. *J. Mol. Biol.* 149:657–707.

Opella, S. J., P. L. Stewart, and K. G. Valentine. 1987. Protein structure by solid-state NMR spectroscopy. *Q. Rev. Biophys.* 19:7–49.

Potel, M. J., T. E. Wellems, R. J. Vassar, B. Deer, and R. Josephs. 1984. Macrofiber structure and the dynamics of sickle cell hemoglobin crystallization. *J. Mol. Biol.* 177:819–839.

Rowitch, D. H., G. J. Hunter, and R. N. Perham. 1988. Variable electrostatic interaction between DNA and coat protein in filamentous bacteriophage assembly. *J. Mol. Biol.* 204:663–674.

Stubbs, G., and L. Makowski. 1982. Coordinated use of isomorphous

replacement and layer-line splitting in the phasing of fiber diffraction data. Acta Crystallogr. A38:417–425.

Torbet, J., and G. Maret. 1979. Formation of highly oriented specimens of filamentous bacteriophage in a magnetic field. *J. Mol. Biol.* 134:843–845.

Vassar, R. J., M. J. Potel, and R. Josephs. 1982. Studies of the fiber to crystal transition of sickle cell hemoglobin in acidic polyethylene glycol. *J. Mol. Biol.* 157:395–412.

Wachtel, E. J., F. J. Marvin, and D. A. Marvin. 1976. Structural transition in a filamentous protein. *J. Mol. Biol.* 107:379–383.

Weisel, J. W., C. Nagaswami, and L. Makowski. 1987. Twisting of fibrin fibers limits their radial growth. *Proc. Natl. Acad. Sci. USA.* 84:8991–8995.

Zimmerman, K., H. Hagedorn, C. C. Heuck, M. Hinrichsen, and H. Ludwig. 1986. The ionic properties of the filamentous bacteriophages Pf1 and fd. *J. Biol. Chem.* 261:1653–1655.